Clinical and Experimental Medicine (2025) 25:180
https://doi.org/10.1007/s10238-025-01700-4

RESEARCH

Prognostic implication of six m6A-modulated genes signature in the ferroptosis for hepatocellular carcinoma patients

Yu He[1] · Zhilin Zou[2] · Zuyong Lan[3] · Ming Chang[4] · Xiao Zhang[5] · Risheng Lin[5] · Wen Zhang[5] · Guangtao Zhang[2] · Ting Wang[2] · Erbao Chen[2]

Received: 3 March 2025 / Accepted: 15 April 2025

Abstract

Hepatocellular carcinoma (HCC) remains one of the most prevalent and lethal malignancies worldwide, with survival rates still falling short of expectations. Emerging evidence highlights the pivotal roles of both m6A methylation and ferroptosis-related genes (FRGs) in HCC progression. However, the prognostic significance of m6A-modulated FRGs remains largely unexplored. In this study, we developed a novel prognostic signature based on m6A-regulated FRGs, identifying six key genes (VEGFA, FANCD2, ZFP69B, EIF2S1, SLC7A11, and SRXN1) through multivariate and LASSO Cox regression analyses. A high m6A-FRGs score was strongly associated with poor prognosis, and multivariate analysis confirmed it as an independent prognostic factor. Notably, the high-risk group exhibited increased expression of immune checkpoint genes and a higher frequency of gene mutations. Functional assays further demonstrated that silencing ZFP69B significantly suppressed liver cancer cell proliferation, migration, and invasion. Clinical validation in 144 HCC samples revealed that elevated ZFP69B expression correlated with worse patient outcomes. Moreover, qPCR analysis confirmed CLSPN and HNRNPR as downstream targets of ZFP69B. Collectively, our findings establish the m6A-FRGs signature as a powerful prognostic tool for HCC and identify ZFP69B as a promising therapeutic target, warranting further investigation.

Keywords Hepatocellular carcinoma · Ferroptosis · M6-methyladenosine · ZFP69B · Immunotherapy · Prognostic signature

Yu He, Zhilin Zou and Zuyong Lan have contributed equally to this work.

✉ Ting Wang
wangtingofsmu@163.com

✉ Erbao Chen
ebchen17@fudan.edu.cn

Guangtao Zhang
haitao161@163.com

1 Institute of Modern Biology, Nanjing University, Nanjing 210008, China

2 Department of Hepatobiliary and Pancreatic Surgery, Peking University Shenzhen Hospital, Shenzhen 518036, Guangdong, China

3 Department of Gastrointestinal Surgery, Changde Hospital, Xiangya School of Medicine, Central South University (The First People's Hospital of Changde City), Changde 415000, Hunan, China

4 Xiangyang Central Hospital, Affiliated Hospital of Hubei University of Arts and Science, Xiangyang 441000, Hubei, China

5 School of Medicine, Southern University of Science and Technology, Shenzhen 518055, Guangdong, China

Abbreviations

TCGA	The Cancer Genome Atlas
LIHC	Liver hepatocellular carcinoma
GEO	Gene Expression Omnibus
FRG	Ferroptosis-related genes
RNA-seq	RNA sequencing
FDR	False discovery rate
GO	Gene ontology
KEGG	Kyoto Encyclopedia of Genes and Genomes
OS	Overall survival
LASSO	Least absolute shrinkage and selection operator
ROC	Receiver operating characteristic
HR	Hazard ratio
CI	Confidence interval
AUC	Area under curve
CDF	Cumulative distribution function
PCA	Principal component analysis
HCC	Hepatocellular carcinoma
MDSC	Myeloid-derived suppressor cells

Published online: 27 May 2025

DC Dendritic cell
95% CI 95% Confidence interval

Introduction

Hepatocellular carcinoma (HCC) is a common and highly lethal malignant tumor worldwide [1]. Owing to the lack of specific clinical symptoms in the early stages, most patients are diagnosed at an advanced stage, often with intrahepatic metastases already present. Consequently, the 5-year survival rate remains extremely poor (approximately 10–20%), primarily due to the tumor's high invasiveness and frequent metastasis [2]. Currently, no single prognostic gene is sufficient to fully capture the complexity of HCC progression. For patients with advanced HCC who are ineligible for curative liver resection, a multidisciplinary treatment strategy is critical for improving clinical outcomes [3]. In recent years, systemic therapies for advanced HCC have undergone significant advancements. The phase III IMbrave150 trial established the combination of atezolizumab and bevacizumab as the new standard first-line treatment, demonstrating marked improvements in overall survival (OS) and progression-free survival (PFS) compared to sorafenib [4]. Furthermore, dual immunotherapy with durvalumab and tremelimumab, has emerged as an additional effective first-line regimen [5]. In parallel with therapeutic innovation, the identification of reliable biomarkers—such as the neutrophil-to-eosinophil ratio (NER)—has gained attention for their potential to guide personalized treatment decisions [6]. In addition, to further improve prognostication in HCC, several gene expression-based signatures have been developed. These include an autophagy-related gene signature [7], an eleven-gene stemness-related signature [8], and a five-gene metastasis-related mRNA signature [9]. Integrative research has revealed that HCC exhibits high heterogeneity at the genomic, transcriptomic, proteomic, and metabolomic levels, and is tightly associated with distinct cellular pathways. Only a precise molecular signature can help HCC patients avoid unnecessary or potentially harmful treatments. Therefore, it is essential to elaborate on the natural history of HCC in combination with clinical characteristics. The development of novel signatures that incorporate more effective prognostic markers and therapeutic targets is urgently needed.

N6-methyladenosine (m6A), the most abundant internal modification in eukaryotic mRNA, is a key post-transcriptional modification that regulates RNA translation, splicing, stability, degradation, and other critical aspects of mRNA metabolism [10]. The biological process of m6A modification is reversible and dynamic, and includes methyltransferases, demethylases, and signal transducers, which are also referred to as "writers," "erasers," and "readers," respectively. Writers, such as METTL3 and METTL14, can increase m6A levels by forming a methyltransferase complex [11], while erasers, including ALKBH5 and FTO, catalyze the removal of m6A modifications through demethylation [12]. Unlike writers and erasers, readers are a class of RNA-binding proteins, such as HNRNPC, YTHDF1, YTHDC2, and YTHDC1, that can recognize m6A modifications and interpret these marks to mediate downstream functional outcomes. Recent studies have suggested that aberrant m6A modifications exert a critical impact on the development and progression of hepatocellular carcinoma (HCC). For example, YTHDF1 drives hypoxia-induced autophagy [13] within the tumor microenvironment. METTL3 promotes HCC growth and metastasis by suppressing SOCS expression in an m6A-dependent manner [14], whereas ALKBH5 suppresses cancer malignancy [15]. However, the role of m6A-modulated genes in relation to HCC prognosis remains poorly understood and requires further elucidation.

Since its first report and definition in 2012, ferroptosis has been recognized as a novel form of regulated cell death, distinct from apoptosis, necrosis, and autophagy. As a unique mode of cell death, ferroptosis participates in multiple essential mechanisms involved in various cancer-related pathways, such as autophagy signaling [16], reactive oxygen species (ROS) metabolism [17], TP53 signaling [18], and MAPK signaling [19]. Up to now, several ferroptosis inducers have been approved for clinical application by the U.S. Food and Drug Administration [20]; thus, ferroptosis-based therapy has attracted considerable attention in cancer treatment. Unfortunately, to the best of our knowledge, the endogenous interaction between m6A status and ferroptosis regulators remains unknown. Thus, exploring the regulatory network of m6A-modulated ferroptosis-related genes (m6A-FRGs) in the development of HCC may provide valuable insights for prognostic prediction and clinical intervention.

Consequently, m6A, a critical biological mechanism in RNA modulation, and ferroptosis, an important form of regulated cell death, may present a promising area for cancer therapy. Our understanding of the regulation of ferroptosis and the m6A process has increased considerably in the last decade. However, little is known about the precise interaction between m6A status and ferroptosis-related gene expression in HCC, and nothing is known yet about its prognostic value in HCC. In the present study, we identified the m6A-related ferroptosis-related genes (FRGs) expression from The Cancer Genome Atlas (TCGA) and analyzed their prognostic value in liver hepatocellular carcinoma (LIHC). Subsequently, we identified six m6A-related ferroptosis-related genes through least absolute shrinkage and selection operator (LASSO) regression analysis. This model comprised a novel m6A-FRGs prognostic signature, which could accurately predict the prognosis of HCC patients. Subsequent multivariate analysis identified that the m6A-FRGs

was an independent indicator for HCC prognosis. Additionally, the m6A-FRGs status was positively associated with immune checkpoint levels. Finally, the m6A-FRGs signature was validated using a cohort from the International Cancer Genome Consortium (ICGC).

Among the m6A-regulated ferroptosis-related genes identified, we focused on Zinc Finger Protein 69B (ZFP69B), a zinc finger transcription factor known to participate in DNA binding and protein–protein interactions. Unlike well-characterized ferroptosis regulators (e.g., SLC7A11), the m6A-mediated regulation of ZFP69B in ferroptosis remains largely unexplored. Clinical analyses revealed a significant association between ZFP69B overexpression and poor prognosis in HCC patients. Collectively, these findings suggest that ZFP69B may serve as a novel m6A-dependent regulator of ferroptosis with promising translational implications for HCC management.

We aim to investigate the potential role of ZFP69B in HCC by examining its expression in clinical liver cancer samples and evaluating its effects on cell proliferation, migration, and invasion in vitro.

Materials and methods

Data acquisition

Transcriptional profiling data of 374 HCC samples and 50 normal tissues, along with clinical characteristics (9 out of 374 patients in the TCGA dataset were removed due to lack of information of survival) were downloaded from the TCGA LIHC database (http://portal.gdc.cancer.gov/repository). Besides, m6A-related genes were obtained from the m6a2target dataset (http://m6a2target.canceromics.org/#/) [21]. Ferroptosis-related genes were acquired from the FerrDb database (http://zhounan.org/ferrdb/) [22]. HCC cohort (n = 243) were downloaded from International Cancer Genome Consortium (ICGC) (https://dcc.icgc.org/) for external validation to test the predictive reliability of the model.

Identification of significantly different expressed genes and functional enrichment analysis

The "limma" package in R software was applied to screen differentially expressed genes between HCC and normal tissues. The thresholds were set at $|\log_2 \text{fold change}| > 1$ and false discovery rate (FDR) < 0.05. ClusterProfiler v4.0 package was utilized to functional annotation: The Gene Ontology (GO) function and Kyoto Encyclopedia of Genes and Genomes (KEGG) pathway.

Consensus clustering analysis

According to the expression of prognostic m6A-FRGs in HCC, all cases in the LIHC cohort were clustered into subgroups by the R package "ConsensusClusterPlus". Then, the Kaplan–Meier survival analysis was performed through the R package "survival" to assess the statistical difference of OS between clusters.

Development of the m6A-FRGs prognostic model

Multivariate cox regression analysis was applied to assess the statistical significance between the m6A-FRGs and the OS of HCC patients. The m6A-related FRGs with prognostic significance ($p < 0.05$) in the TCGA dataset were used to screen into a LASSO Cox regression. The analysis achieved by using the "glmnet" package in R software and then generated crucial genes for m6A-related ferroptosis-related genes (m6A-FRGs) prognostic signature. The formula was calculated with the combinational of the normalized gene expression weighted by their corresponding regression coefficients: Risk score = (Expr of Gene1* Coef of Gene1) + (Expr of Gene2*Coef of Gene2) + … + (Expr of Gene-n* Coef of Gene-n), with "Expr" referring to transcriptional expression of m6A-FRGs "Coef" referring to corresponding regression coefficient calculate by LASSO.

Assessment of the prognostic value m6A-FGR prognostic signature

Kaplan–Meier survival analysis with log-rank test was applied to assess the survival relationship between m6A-FRGs signature and the OS of HCC patients. The "survivalROC" R package was used to time-dependent receiver operating characteristic (ROC) analysis to evaluate the predictive accuracy of m6A-FRGs signature. Principal components analysis (PCA) was applied to describe the distribution patterns of three clusters. Multivariate cox was performed to confirm the independency of the prognostic m6A-FRGs.

Correlations between model and immune checkpoint genes and microenvironment profiles

We compared the expression of immune checkpoint genes (programmed cell death 1, PD-1; Programmed cell death 1 ligand 1, PD-L1; T-cell immunoglobulin and mucin domain 3, TIM3; lymphocyte-activation gene 3, LAG3; T cell immunoreceptor with immunoglobulin and ITIM domain, TIGIT) in different risk groups. The fraction of 19

microenvironment components infiltrated in tumor tissue was assessed using the previous literature [23].

Cell culture and transfection

The Huh7 and HepG2 cell lines were obtained from Guangzhou Cellcook Biotech Co, Ltd. (Guangdong, China). Both cell lines were cultured in DMEM (Gibco, USA), supplemented with 10% fetal bovine serum and 1% Penicillin/Streptomycin, and maintained at 37 °C in a 5% CO2 incubator. Mycoplasma contamination was regularly tested using the Mycoplasma Detection Kit (Solarbio, Beijing, China). ZFP69B siRNA and universal negative control siRNA were purchased from General BioL (China). Lipofectamine RNAiMAX transfection reagent and OPTI-MEM medium were obtained from Thermo Fisher (USA).

Clinical liver cancer patient samples

144 HCC tissue samples were collected from patients who underwent curative hepatectomy at Peking University Shenzhen Hospital between January 2015 and December 2018. These samples were used to construct tissue microarrays (TMAs). Overall survival (OS) was defined as the time from the date of surgery to either death or the end of the follow-up period (December 2021). Disease-free survival (DFS) was measured from the date of surgery to the date of recurrence or the last follow-up. All cases were independently reviewed by two pathologists. This study was conducted in accordance with the Declaration of Helsinki. The use of clinical specimens, patient characteristics, and follow-up data for research purposes was approved by the ethics committee of Peking University Shenzhen Hospital. Informed consent was obtained from all patients prior to surgery. Ethics approval (IRB# 2023-072).

Cell viability assay and colony formation assay

Cell suspensions (3×10^3 cells per well) were seeded into 96-well plates, and cell proliferation was measured at 24, 48, and 72 h. Then, 10 µl of CCK-8 reagent (Dojindo, Japan) was added to each well, and the plates were incubated for 2 h. The absorbance at 450 nm was then measured using a microplate reader.

A total of 1×10^3 cells were seeded into 6-well plates and cultured for 14 days, with medium changes every 3 days. Afterward, the plates were washed three times with PBS, fixed with 4% paraformaldehyde, and stained with 1% crystal violet. Colony numbers were then counted and recorded.

Cell migration and invasion assays

Migration and invasion assays were performed using Transwell chambers, with and without Matrigel (BD, USA) coating. For migration assays, 6×10^4 cells were added to the upper chambers without Matrigel, and for invasion assays, 1.2×10^5 cells were added to the chambers with Matrigel. A total of 800 µl of medium containing 20% FBS was placed in the lower chamber. After 24 h of incubation, cells on the lower surface of the membrane were fixed with 4% paraformaldehyde for 20 min, then stained with 1% crystal violet for 15 min. The number of migratory or invasive cells was counted by examining three randomly selected microscopic fields per well using a light microscope.

Immunohistochemical staining of the TMA

Immunohistochemical staining was performed as previously described [24]. In brief, TMA slides were first dewaxed in xylene for 10 min and rehydrated using graded ethanol. Antigen retrieval was done using a citric acid buffer (pH 6.0) for 20 min. To block endogenous peroxidase activity, the sections were treated with 3% hydrogen peroxide for 5 min. The slides were then incubated overnight at 4 °C with rabbit anti-ZFP69B antibody (1:100 dilution; Signalway Antibody; 39824). Afterward, they were incubated with secondary antibodies for 1 h at 37 °C. The slides were stained with DAB for 2 min in the dark, followed by hematoxylin staining for 2 min. Finally, the slides were dehydrated with graded alcohol, mounted with neutral balsam, and visualized using CaseViewer2.4 and Quant Center2.1 (3DHISTECH, Hungary).

qRT-PCR assay

Total RNA was extracted from cells using 1 mL of Trizol (Invitrogen, USA), followed by reverse transcription using Prime-Script RT Master Mix (Vazyme, China). Quantitative Reverse Transcription Polymerase Chain Reaction (qRT-PCR) was conducted with SYBR Green Realtime PCR Master Mix (Vazyme, China). Each experiment was independently repeated three times.

Statistical analysis

All data were calculated statistically by R software and GraphPad Prism 9. The OS of the high- and low- risk groups were compared via the Kaplan–Meier method with a log-rank test. A hazard ratio (HR) and a 95% confidence interval (CI) were assessed by univariable and multivariate Cox regression analysis. A p value of less than 0.05 was considered to be statistically significant ($*p<0.05$, $**p<0.01$, $***p<0.001$, $****p<0.0001$).

Results

Identification of 55 m6A-related genes in the ferroptosis in HCC patients

The detailed flowchart for risk model signature construction and subsequent system analyses is shown in Fig. 1. The transcriptional gene expression data were used to analyze this study. We first obtained 259 FRGs from the FerrDb, 14,152 m6A-related modification genes specified in HCC cell lines from the m6A2target and 28210 differentially expressed genes were downloaded for model construction in the TCGA dataset (Supplementary Excel 1–3). Next, combined with clinical information, univariate cox regression analysis was used to screen out prognostic indicators. Venn diagram showed that 55 genes overlapped among the four groups combined with gene differential expression analysis (Fig. 2A). The results suggested that 55 genes in TCGA cohort were remarkably associated with the overall survival (OS) ($p < 0.05$). There were 49 genes up-regulated and 6 genes were down-regulated in the tumor compared with the normal tissues (Fig. 2B). To reveal the molecular mechanism behind the 55 FRGs, the top three terms BP for GO analysis were cellular response to chemical stress, cellular response to oxidative stress, and response to oxidative stress in the Fig. 2C. The top three CC terms for GO analysis were autophagosome, autolysosome and melanosome. The top three MF terms for GO analysis were ferric iron binding, antioxidant activity and RNA polymerase II-specific DNA binding. For KEGG pathway analysis, the cancer- or ferroptosis-related KEGG pathways were remarkably enriched in the high-risk group (Fig. 2C, D), such as Chemical carcinogenesis-reactive oxygen species, Ferroptosis, Autophagy-animal, Necroptosis, Hepatocellular carcinoma, Mitophagy-animal, HIF-1 signaling pathway and bladder cancer, MAPK signaling pathway, and Apoptosis.

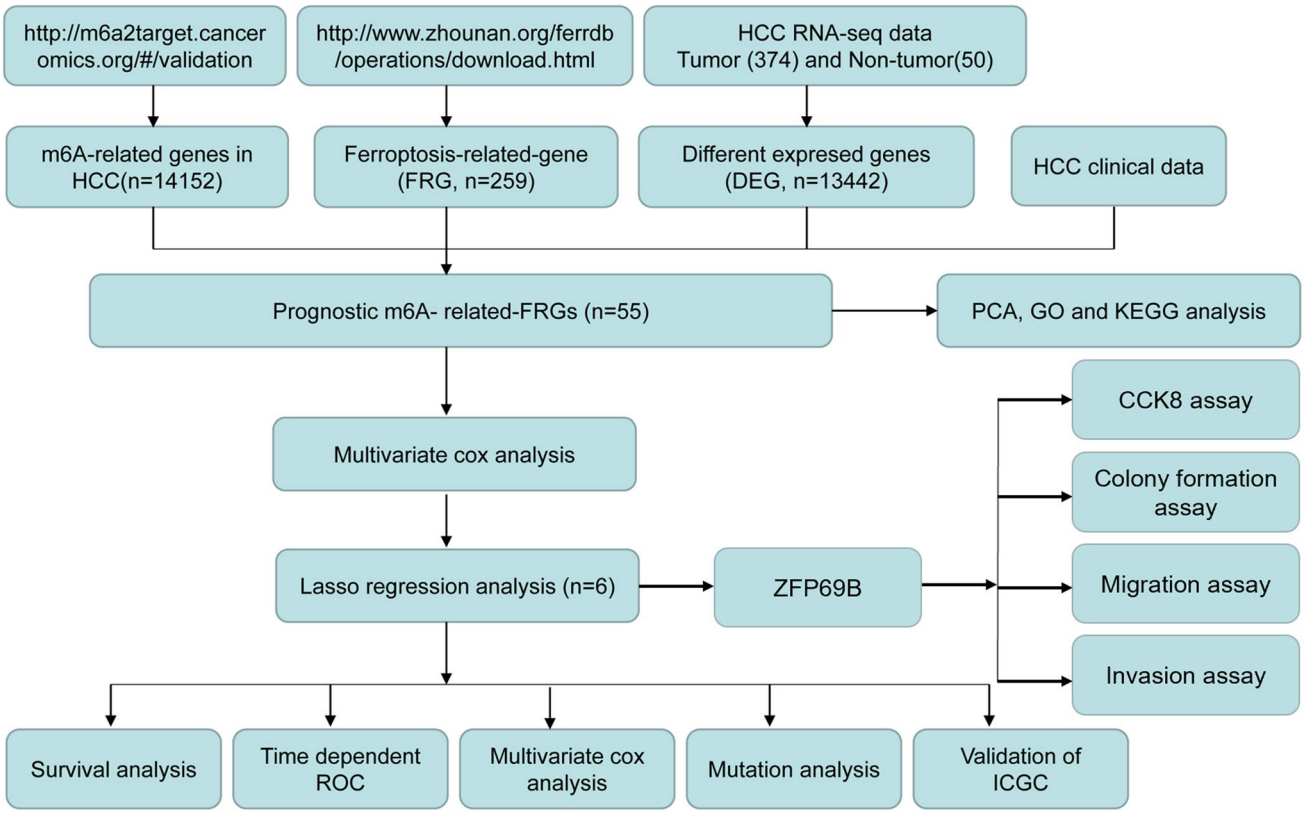

Fig. 1 Flow chart of this study. Overview of the comprehensive analysis. We first obtained 259 FRGs and 14,152 m6A modification genes in the TCGA dataset. Then, 55 genes were identified as prognostic factors after univariate cox regression and had been selected for further analysis. We performed LASSO Cox regression analysis to further filter a model that contained 6 FRGs and have an excellent prognostic efficacy. Finally, enrichment analysis and validation experiments were used to explore the functions of these genes in HCC. Additionally, among these 6 genes, ZFP69B was identified as a key gene, and its function was validated through in vitro experiments. Abbreviations: FRG, ferroptosis-related gene; TCGA, the Cancer Genome Atlas; LASSO, least absolute shrinkage and selection operator; HCC, hepatocellular carcinoma

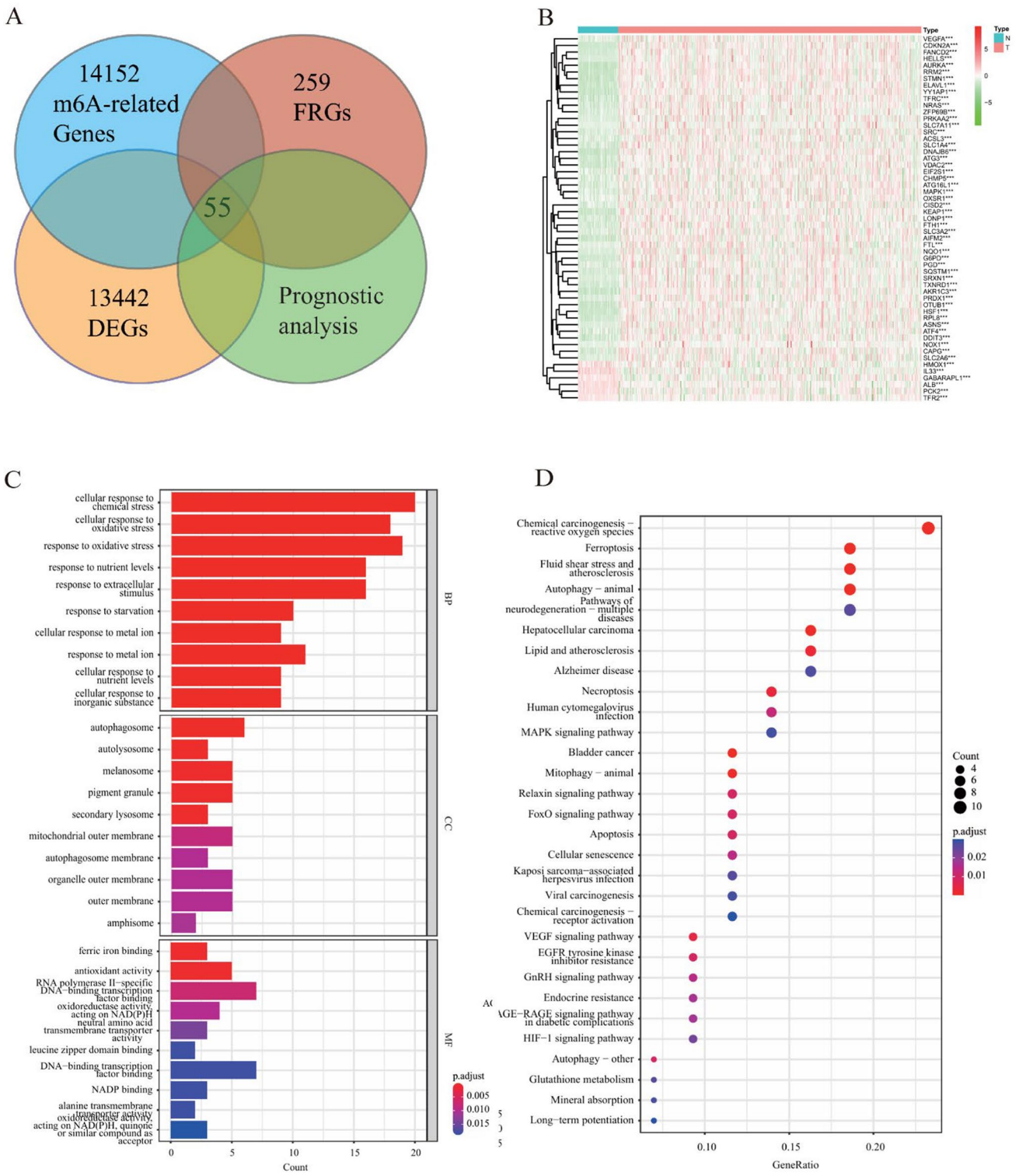

Fig. 2 Identification of 55 FRGs by combined analysis. **A** A total of 55 prognostic genes were identified and were associated with ferroptosis and m6A status in the TCGA cohorts. **B** A heatmap showing the expressions of the 55 prognostic genes in tumors and normal tissues in the TCGA cohorts. Green represents downregulation, and red represents upregulation of genes. **C** GO annotation: Top 10 enriched biological processes, molecular functions, cellular components. and **D** KEGG pathway enrichment analysis of the 55 genes revealed key molecular potential pathways potentially involved in HCC progression. Abbreviations: FRG, ferroptosis-related gene; TCGA, the Cancer Genome Atlas; HCC, hepatocellular carcinoma; GO, Gene Ontology; KEGG, Kyoto Encyclopedia of Genes and Genomes

Profile of 55 m6A-relatad genes in the ferroptosis among HCC

According to the profile of these 55 genes, we used the consensus clustering analysis to assess the significance of m6A-FRGs in the progression of HCC by dividing all the cases into different clusters. The cumulative distribution function (CDF) of different clustering methods from k = 2 to 9 and the relative changes of the area under CDF curves are shown in Fig. 3A, B. The corresponding sample distribution is shown in Fig. 3C. Considering the increase in CDF and consistent expression of m6A-FRGs in HCC, two clusters were determined with 220 and 149 cases in cluster 1 and 2, respectively (Fig. 3D). PCA analysis revealed a significant difference in gene expression profiles between these two clusters (Fig. 3E). And the results of KM plotter showed that these two clusters had distinct survival (Fig. 3F). As for the clinical characteristics, no significant differences on T stage, N stage, M stage, gender, or age were observed between the two clusters (Fig. 3G).

Construction of a prognostic signature model based on m6A-FRGs in HCC

To further reduce the candidate genes in the Lasso analysis, six genes were identified as prognostic factors by multivariate Cox regression ($p < 0.1$), then LASSO analysis was applied to the 6 m6A related-FRGs to generate a prognostic signature (m6A-FRGs). (Fig. 4A, B). Eventually, 6 genes (EIF2S1, VEGFA, FANCD2, SLC7A11, ZFP69B, SRXN1) were enrolled to construct the risk signature according to the minimum criteria of LASSO. Based on the coefficients, the following formula was used to calculate the risk score: The expression of EIF2S1 * 0.4685 + FANCD2 * 0.1341 + SLC7A11 * 0.2265 + SRXN1*0.3075 + VEGFA *0.1249 + ZFP69B*0.6225. The optimal cutoff value for the m6A-FRGs risk score was identified using the surv_cutpoint function from the survminer R package (version 0.5.0), which employs maximally selected rank statistics to maximize survival differences between high- and low-risk groups. This approach iteratively evaluates potential thresholds to find the value with the highest log-rank test statistic. These data show that the risk signature could be a novel prognostic predictor for HCC. As illustrated in Fig. 4C, the OS of the high-score group was worse than that of low-score group based on the optimal m6A-FRGs cutoff value. Time-dependent ROC analysis was performed to evaluate the prognostic accuracy of m6A-FRGs. As shown in Fig. 4D, the area under the curve (AUC) for 1-, 3-, 5-year OS reached 0.76, 0.68, and 0.66, respectively, suggesting a powerful predictive value of the m6A-FRGs.

Association of gene signature with clinicopathological characters in HCC

To further investigate the clinical characteristics between m6A-FRGs, we observed that there were no obvious differences between low- and high-risk groups regarding clinical N stage, M stage, gender, and age. However, there were statistically significant differences in T stage, Stage, and fustat (Fig. 5A). Regarding the T stage, with an increase in the stage level, the risk score also increased. Significant differences were observed between T1 stage and T2, T3 stages, with p values of 0.041 and 0.00084, respectively. However, there were no significant statistical differences between T1 stage and T4 stage (Fig. 5B). In terms of Stage, a significant difference in risk scores was observed between Stage 1 and Stage 3 ($p = 0.00016$), while no significant differences were found between Stage 1 and Stage 2 ($p = 0.06$) or Stage 1 and Stage 4 ($p = 0.91$) (Fig. 5C). In the univariate cox analysis, Stage, T stage, M stage and risk score were remarkably correlated with OS (Fig. 5D). Multivariate cox analysis presented that only m6A-FRGs risk signature remained significantly correlated with OS, which indicating that m6A-FRGs signature could serve as an independent prognostic predictor for OS of HCC (Fig. 5E).

Immune microenvironment and gene mutations associated with m6A-modulated ferroptosis in hepatocellular carcinoma

At present, immunotherapy has become an important treatment for prolonging the survival of multiple types of cancers. The correlation between m6A-FRGs and the microenvironment subtypes in the TCGA-LIHC dataset was investigated. The distributions of different microenvironment signatures in TCGA-LIHC were obtained from previous literature [23]. The high-risk group comprised major immune cell associated signatures, such as macrophages, macrophage-DC trafficking, MDSC trafficking, MHCII and MHCI. The high-risk group was also enriched in gene expression signatures defining stromal components, such as matrix remodeling, protumor cytokines, granulocyte traffic and proliferation rate, whereas the high-risk group was negatively associated with the numbers of endothelium and Th2 signature (Fig. 6A). We observed that the high-risk group exhibited a higher level of gene mutation compared with the low-risk group. We noted that the different gene mutations in the high (Fig. 6B) and low (Fig. 6C) risk groups. There were 86 gene mutations with statistically difference between high and low m6A-FRGs score groups (Supplementary Excel 4). Our results revealed that the mutation of TP53 ($p < 0.00001$), DNAH10 ($p = 0.00002$), OBSCN ($p = 0.00292$) and KEAP1 ($p = 0.00331$) was significantly different between

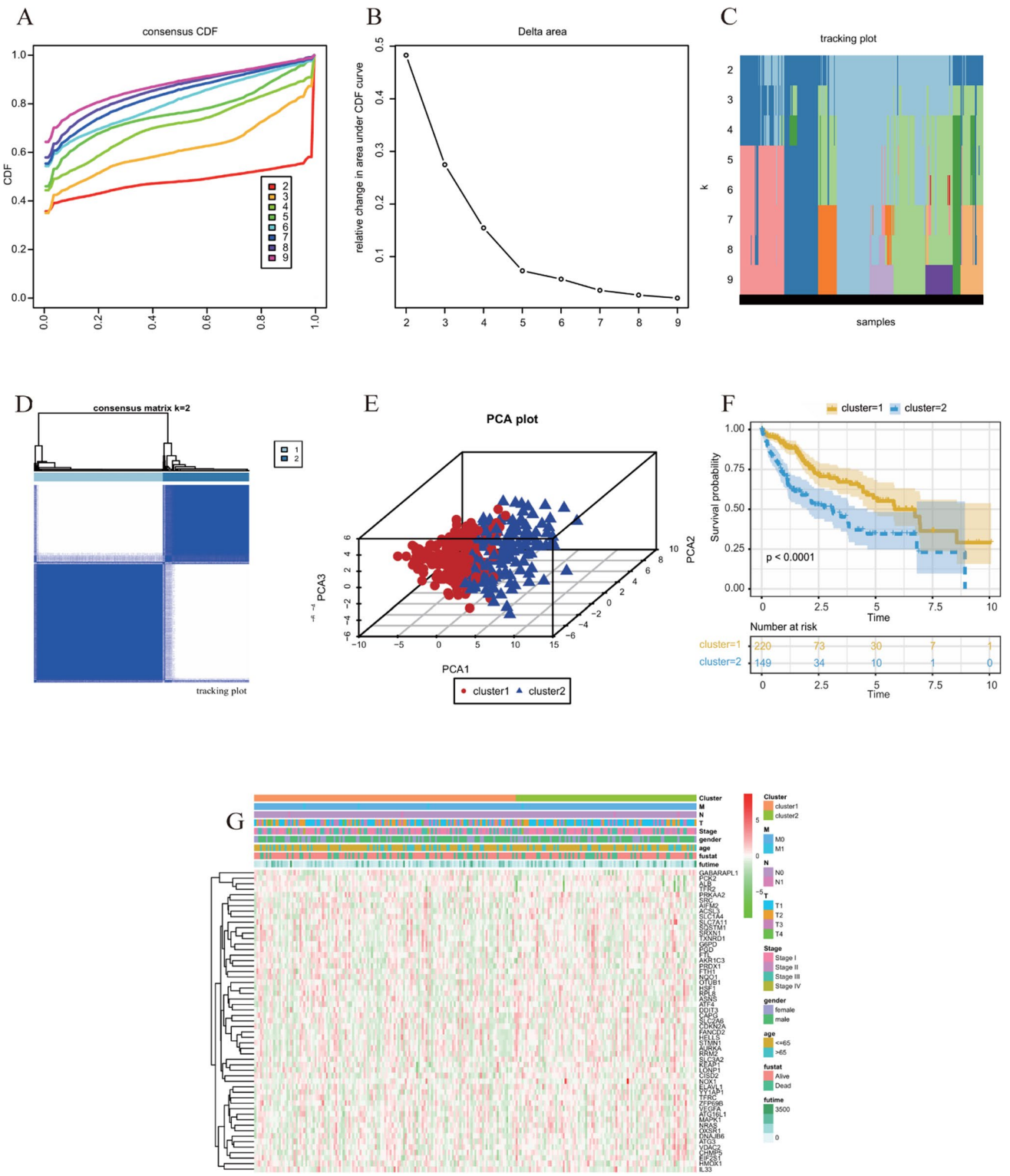

Fig. 3 Consensus clustering analysis of 55 prognostic FRGs in the HCC. **A**–**C** The consensus CDF, relative changes in area under the CDF curves, and tracking plots showed with the index from 2 to 9. **D** The distribution of different clusters with index k = 2. **E** The 2D PCA plots of the TCGA dataset based on the expression of 55 signature genes in different risk groups. **F** There was significant difference about prognosis between two cluster. **G** There were no obvious differences in T stage, N stage, M stage, gender, or age were observed between the two clusters. $*p < 0.05$, $**p < 0.01$, $***p < 0.001$. Abbreviations: FRG, ferroptosis-related gene; PCA, principal component analysis; TCGA, the Cancer Genome Atlas; HCC, hepatocellular carcinoma

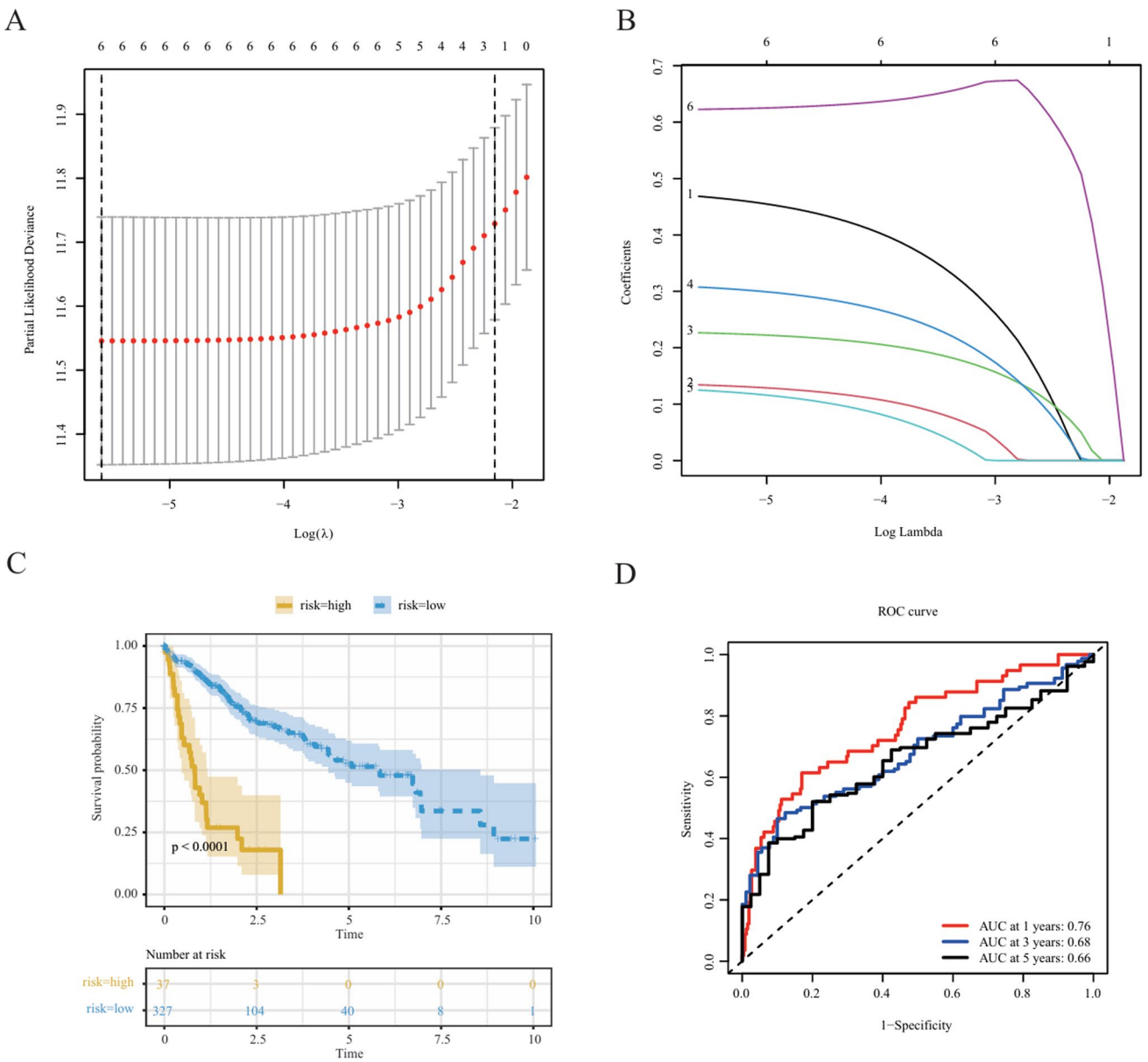

Fig. 4 Construction of a predictive model and m6A-FRGs of HCC. **A**, **B** The LASSO Cox regression model was constructed from the six prognostic genes, and the tuning parameter (lambda) was calculated based on the partial likelihood deviance with tenfold cross-validation. An optimal log value is indicated by the vertical black line in the plot. **C** Survival curves revealed that the subgroup with higher risk had a worse OS rate compared with patients with low-risk subgroup. **D** The AUC of the ROC analysis showed the predicted efficacy of the m6A-FRGs. Abbreviations: FRG, ferroptosis-related genes; HCC, hepatocellular carcinoma; LASSO, least absolute shrinkage and selection operator; OS, overall survival; ROC, receiver operating characteristic; HR, hazard ratio; CI, confidence interval; AUC, area under curve

high and low m6A-FRGs score groups, suggesting that mutation of these genes may be involved in the ferroptosis regulation. Next, we further evaluated the correlation between the m6A-FRGs and the levels of immune checkpoints. The high-risk group had significantly positively associated with higher expression levels of CD276, CD47, CD80, HAVCR2, VTCN1 and TIGIT (Fig. 6D).

Verification of m6A-FRGs in ICGC dataset

We obtained the ICGC datasets for external validation. The heatmap showed that the expression of SLC7A11, SRXN1, VEGFA, EIF2S1, FANCD2 and ZFP69B in the ICGC dataset (Fig. 7A). Kaplan–Meier plotter revealed that the high score of m6A-FRGs can predict worse outcome of HCC

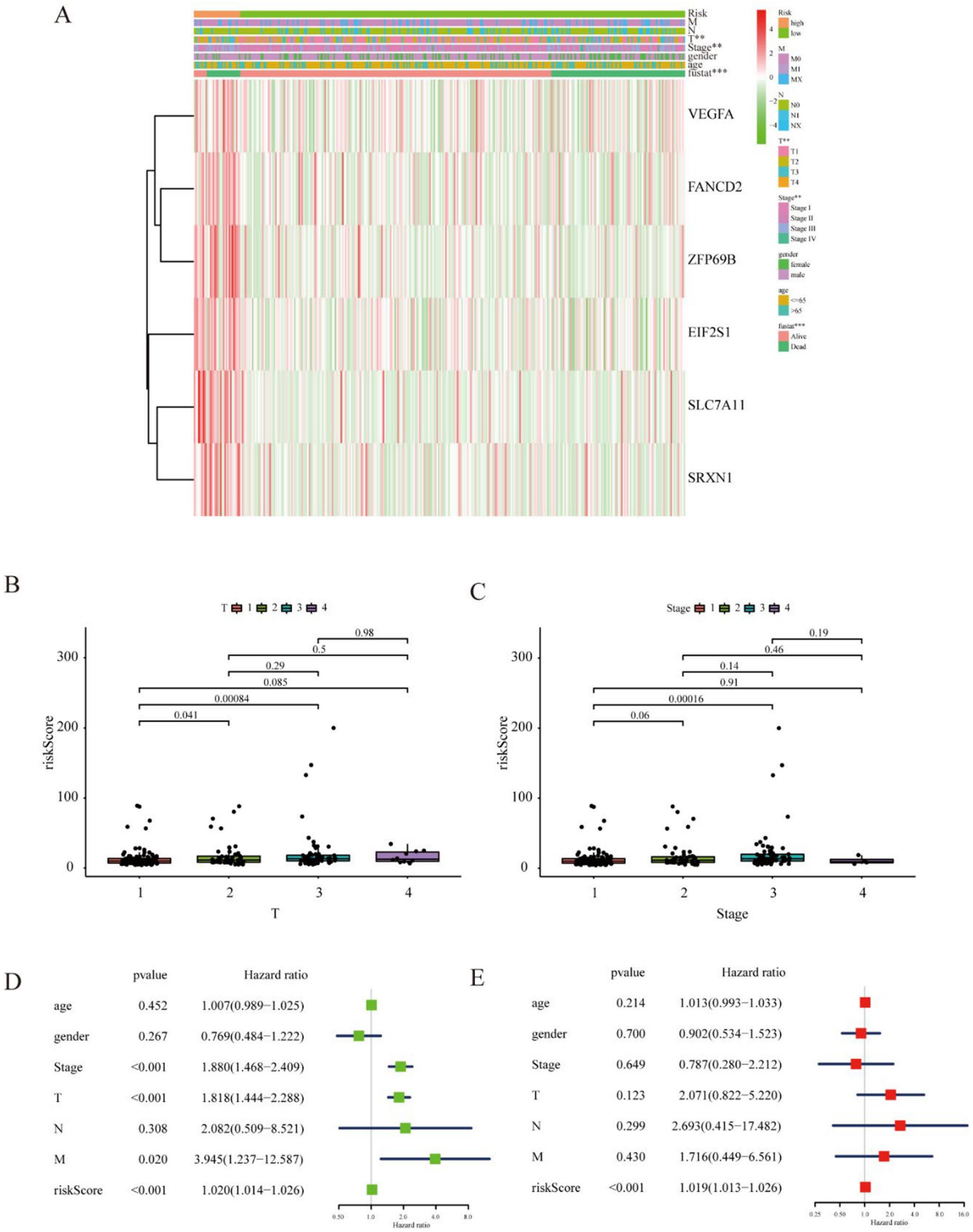

Fig. 5 Clinical significance and prognostic value of m6A. **A** The heatmap showing the relationship between m6A-FRG and clinical characteristics. **B**, **C** The associations between m6A-FRGs and T stage, and Stage. **D** Univariate and **E** multivariate Cox regression analyses for OS in HCC patients. Abbreviations: FRG, ferroptosis-related genes; OS, overall survival; HCC, hepatocellular carcinoma

patients in the ICGC dataset ($p = 0.0016$) (Fig. 7B). The m6A-FRGs was an effective predictor of clinical outcomes in the first three years (Fig. 7C). Furthermore, gender, m6A-FRGs and tumor stage were significantly correlated with OS in the univariate cox analysis (Fig. 7D), and the results of multivariate cox analysis are the same, indicating that m6A-FRGs signature could serve as an independent prognostic predictor for OS of HCC (Fig. 7E).

Silencing of ZFP69B inhibits HCC growth and metastasis in vitro

Due to the fact that SLC7A11, SRXN1, VEGFA, EIF2S1, and FANCD2 have been extensively studied and are known to be closely related to critical biological processes in cancer, such as oxidative stress, angiogenesis, DNA repair, and translational regulation, the study of ZFP69B remains relatively limited. Its functions and specific roles in liver cancer are still unclear. Furthermore, a chi-square analysis was used to compare the ZFP69B levels and clinicopathological features. The results showed that ZFP69B levels were significantly positively associated with AFP levels ($p = 0.025$) and TNM stage ($p < 0.001$) (Table 1). To further investigate the role of ZFP69B, we silenced its expression to observe changes in cell proliferation, migration and invasion. First, we knocked down ZFP69B in Huh7 and HepG2 cells using siRNA. As shown in Fig. 8A, compared to the siRNA-Control, the expression level of ZFP69B was significantly down-regulated at the 48 h after transfection of siRNA-118 and siRNA-119 into the cells. Subsequently, the CCK-8 assay demonstrated that silencing ZFP69B expression with siRNA significantly inhibited the proliferation of Huh7 and HepG2 cells (Fig. 8B). Furthermore, the colony formation assay indicated that the downregulation of ZFP69B substantially suppressed the colony formation ability of Huh7 and HepG2 cells (Fig. 8C). Additionally, silencing ZFP69B could suppress migration and invasion of HepG2 and Huh7 cells (Fig. 8D, E). Taken together, these results have suggested that suppressing the expression of ZFP69B could inhibit the proliferation, migration, and invasion ability of liver cancer cells.

High expression of ZFP69B predicts poor prognosis in liver cancer patients

To explore the effects of ZFP69B on the HCC survival, we stratified 144 cases into two subgroups based on median ZFP69B expression: ZFP69B-high (n = 72) and ZFP69B-low (n = 72). Representative images of high and low ZFP69B expression are shown in Fig. 9A. Kaplan–Meier survival curves indicated that the patients with higher ZFP69B levels had remarkably shorter overall survival (OS) (Fig. 9B). Similarly, patients with higher ZFP69B levels exhibited significantly shorter disease-free survival (DFS) (Fig. 9C).

Downstream targets and pathways associated with ZFP69B

Based on the TCGA LIHC cohort, patients were categorized into two groups: high and low ZFP69B expression. By comparing the gene expression profiles between these groups, we found that 2544 genes were upregulated and 39 genes were downregulated in the high ZFP69B expression group (Fig. 10A). Notably, among these 2544 upregulated genes, those showing the most significant expression changes correlated with ZFP69B—based on the greatest fold-change—were BTBD10, MDC1, DVL3, DCLRE1B, HNRNPR, SART3, CLSPN, EXO5, TCEANC2, and ZMYM1 (Fig. 10B). To investigate whether these ten selected genes are downstream targets of ZFP69B in liver cancer, we performed qPCR assays for validation. In Huh7 cells, ZFP69B was silenced using two siRNAs, and the results demonstrated that CLSPN, BTBD10, HNRNPR, SART3, and EXO5 were downregulated after ZFP69B knockdown (Fig. 10C). In HepG2 cells, CLSPN and HNRNPR were downregulated upon ZFP69B knockdown (Fig. 10D). Combining the results from both liver cancer cell lines, we identified CLSPN and HNRNPR as downstream targets of ZFP69B.

Discussion

Hepatocellular carcinoma (HCC) represents a major global health challenge and contributes substantially to cancer-related mortality worldwide. Despite notable advancements in radical surgical resection and systemic therapies, the long-term prognosis of HCC remains unsatisfactory due to high rates of recurrence and metastasis. Therefore, the identification of reliable prognostic biomarkers is urgently needed to improve risk stratification and guide individualized treatment strategies. In the present study, we comprehensively analyzed transcriptomic profiles and clinical data from publicly available datasets. A total of 259 m6A-related genes associated with the ferroptosis pathway were identified as prognostically significant. Through least absolute shrinkage and selection operator (LASSO) regression analysis, we constructed a novel prognostic signature based on six mRNAs (EIF2S1, VEGFA, FANCD2, SLC7A11, ZFP69B, and SRXN1), referred to as the m6A-FRGs signature. Kaplan–Meier survival analysis and multivariate Cox regression revealed that patients classified into the high-risk

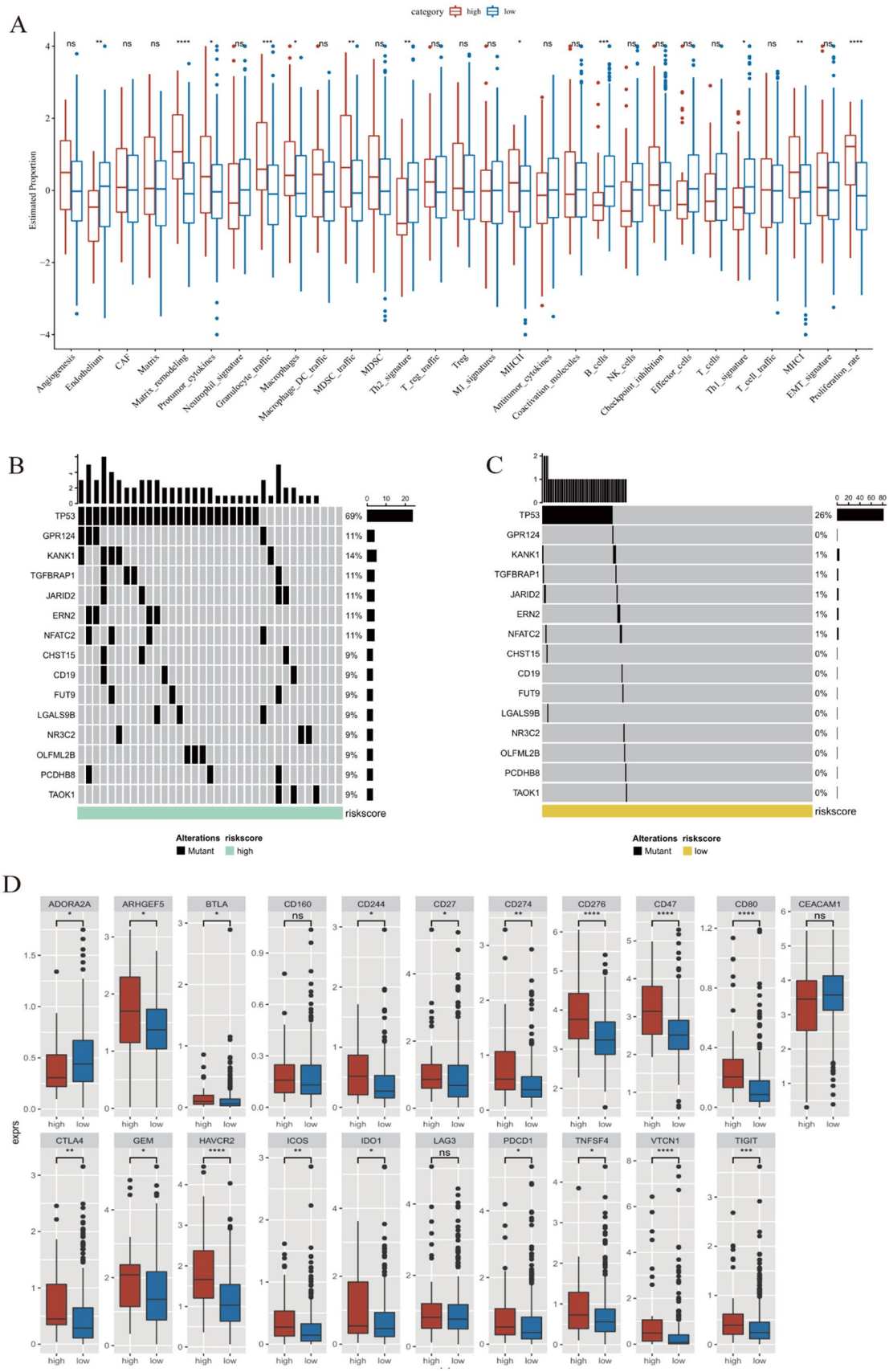
A
category high low
Estimated Proportion
Angiogenesis
Endothelium
CAF
Matrix
Matrix_remodeling
Protumor_cytokines
Neutrophil_signature
Granulocyte_traffic
Macrophages
Macrophage_DC_traffic
MDSC_traffic
MDSC
Th2_signature
T_reg_traffic
Treg
M1_signatures
MHCII
Antitumor_cytokines
Coactivation_molecules
B_cells
NK_cells
Checkpoint_inhibition
Effector_cells
T_cells
Th1_signature
T_cell_traffic
MHCI
EMT_signature
Proliferation_rate
B
TP53 69%
GPR124 11%
KANK1 14%
TGFBRAP1 11%
JARID2 11%
ERN2 11%
NFATC2 11%
CHST15 9%
CD19 9%
FUT9 9%
LGALS9B 9%
NR3C2 9%
OLFML2B 9%
PCDHB8 9%
TAOK1 9%
riskscore
Alterations riskscore
Mutant high
C
TP53 26%
GPR124 0%
KANK1 1%
TGFBRAP1 1%
JARID2 1%
ERN2 1%
NFATC2 1%
CHST15 0%
CD19 0%
FUT9 0%
LGALS9B 0%
NR3C2 0%
OLFML2B 0%
PCDHB8 0%
TAOK1 0%
riskscore
Alterations riskscore
Mutant low
D
ADORA2A
ARHGEF5
BTLA
CD160
CD244
CD27
CD274
CD276
CD47
CD80
CEACAM1
CTLA4
GEM
HAVCR2
ICOS
IDO1
LAG3
PDCD1
TNFSF4
VTCN1
TIGIT
exprs
high low

◂**Fig. 6** Immune signature, tumor mutation profiles, and immune checkpoint expression in m6A-modulated ferroptosis in HCC. **A** The high-risk group comprised major immune cell associated signatures, such as macrophages, Macrophage-DC trafficking, MDSC trafficking, MDSC, Treg trafficking, Treg, MHCII, T cells, MHCI. The high-risk group also were enriched in gene expression signatures defining stromal components, such as matrix remodeling, granulocyte traffic, coactivation molecules, checkpoint inhibition, and proliferation rate, whereas the high-risk group was negatively associated with the numbers of endothelium and Th2 signature. **B** Tumor mutation profiles in the high risk m6A-FRGs. **C** Tumor mutation profiles in the low risk m6A-FRGs. **D** The expression of CD276, CD47, CD80, HAVCR2, VTCN1 and TIGIT were upregulated with significance in the high score of m6A-FRGs. Abbreviations: PD-1, programmed cell death 1; PD-L1, programmed cell death 1 ligand 1; TIM3, T-cell immunoglobulin and mucin domain 3; LAG3, lymphocyte-activation gene 3; TIGIT, T cell immunoreceptor with immunoglobulin and ITIM domain. Abbreviations: MDSC, Myeloid-derived suppressor cells; DC, dendritic cell; FRG, ferroptosis-related genes; TCGA, the Cancer Genome Atlas

group based on this signature exhibited significantly reduced overall survival compared to those in the low-risk group. These findings suggest that the m6A-FRGs model is a promising and robust prognostic indicator for patients with HCC, with potential applications in clinical decision-making and precision oncology.

Specifically, the expression levels of EIF2S1, VEGFA, FANCD2, SLC7A11, ZFP69B, and SRXN1 were found to be significantly elevated in HCC. Notably, among these six genes, EIF2S1 was not only implicated in Xin Li's classification system but also identified as a key component of the endoplasmic reticulum stress-related signature, highlighting its potential importance in HCC progression and prognosis [25]. EIF2S1 has been reported to promote tumorigenesis by enhancing tumor cell proliferation and conferring resistance to apoptosis under hypoxic and nutrient-deprived conditions [26]. However, the role of EIF2S1 in HCC remains to be clarified. Of note, VEGFA promotes the proliferation and migration of vascular endothelial cells, thereby stimulating tumor angiogenesis and ensuring an adequate blood supply for HCC growth and metastasis. Given that HCC is a highly vascularized tumor, elevated VEGFA expression is often associated with increased invasiveness and poor prognosis [27]. FANCD2 may play a crucial role in maintaining genomic stability in HCC by participating in DNA damage repair. Studies have shown that the HCC cell line Huh7 exhibits defects in FANCD2 monoubiquitination and nuclear focus formation, while remaining proficient in RAD51 focus formation. Gene complementation experiments further revealed that this inactivation of the proximal Fanconi anemia (FA) pathway is attributed to defective FANCC function in Huh7 cells. Given that HCC development is closely associated with chronic liver injury, inflammation, and genomic instability, FANCD2 dysfunction may significantly contribute to disease progression [28]. The METTL9–SLC7A11 axis has been identified as a critical pathway promoting HCC progression by inhibiting ferroptosis. SLC7A11 maintains intracellular glutathione (GSH) levels, thereby protecting cells from oxidative stress and ferroptosis. Its high expression is closely associated with advanced HCC stages and poor patient prognosis [29]. ZFP69B expression is significantly elevated in gastric cancer compared to normal tissues and has been proposed as a potential prognostic indicator in this context [30]. However, the role of ZFP69B in HCC remains uncharacterized.

We divided the patients into two risk groups based on the median cutoff of the m6A-FRGs score. Patients in the high-risk group had significantly shorter overall survival (OS) than those in the low-risk group. The time-dependent ROC curve demonstrated that the m6A-FRGs signature had high predictive accuracy for patient prognosis, particularly for 1-year OS prediction. Multivariate Cox regression analysis confirmed that the m6A-FRGs signature is an independent prognostic biomarker for HCC. Furthermore, patients in the high-risk group exhibited increased immune cell infiltration and higher expression levels of immune checkpoint proteins, including PD-1, PD-L1, TIM-3, LAG-3, and TIGIT. Notably, the high m6A-FRGs group also showed a significantly higher mutation rate in key tumor suppressor genes, such as TP53. These findings suggest that HCC patients with higher risk scores may derive greater benefit from immunotherapy.

Moreover, recent advancements in HCC immunotherapy have highlighted the potential of immune checkpoint inhibitors (ICIs) like pembrolizumab, nivolumab, and atezolizumab. However, clinical trials assessing single-agent ICIs have reported disappointing results in HCC, underscoring the need for better predictive biomarkers of response. In contrast, combination therapies, such as the combination of atezolizumab (PD-L1 inhibitor) and bevacizumab (anti-VEGF agent), have shown remarkable clinical benefits. These findings emphasize the importance of understanding biomarkers such as PD-L1 expression, tumor mutational burden (TMB), and microsatellite instability (MSI) in predicting therapeutic outcomes.

However, several important questions remain unanswered regarding the use of ICIs in HCC. First, only a subset of patients benefits from immunotherapy, which raises concerns about the lack of reliable biomarkers. Therefore, a more comprehensive understanding of potential biomarkers, including those identified in this study, is critical to optimizing treatment strategies. In addition, the heterogeneity in clinical trial designs, patient populations, and treatment regimens across studies has led to inconsistent results, further complicating the evaluation of immunotherapy in HCC.

We further validated the expression and prognostic value of the novel m6A-FRGs signature in an external dataset.

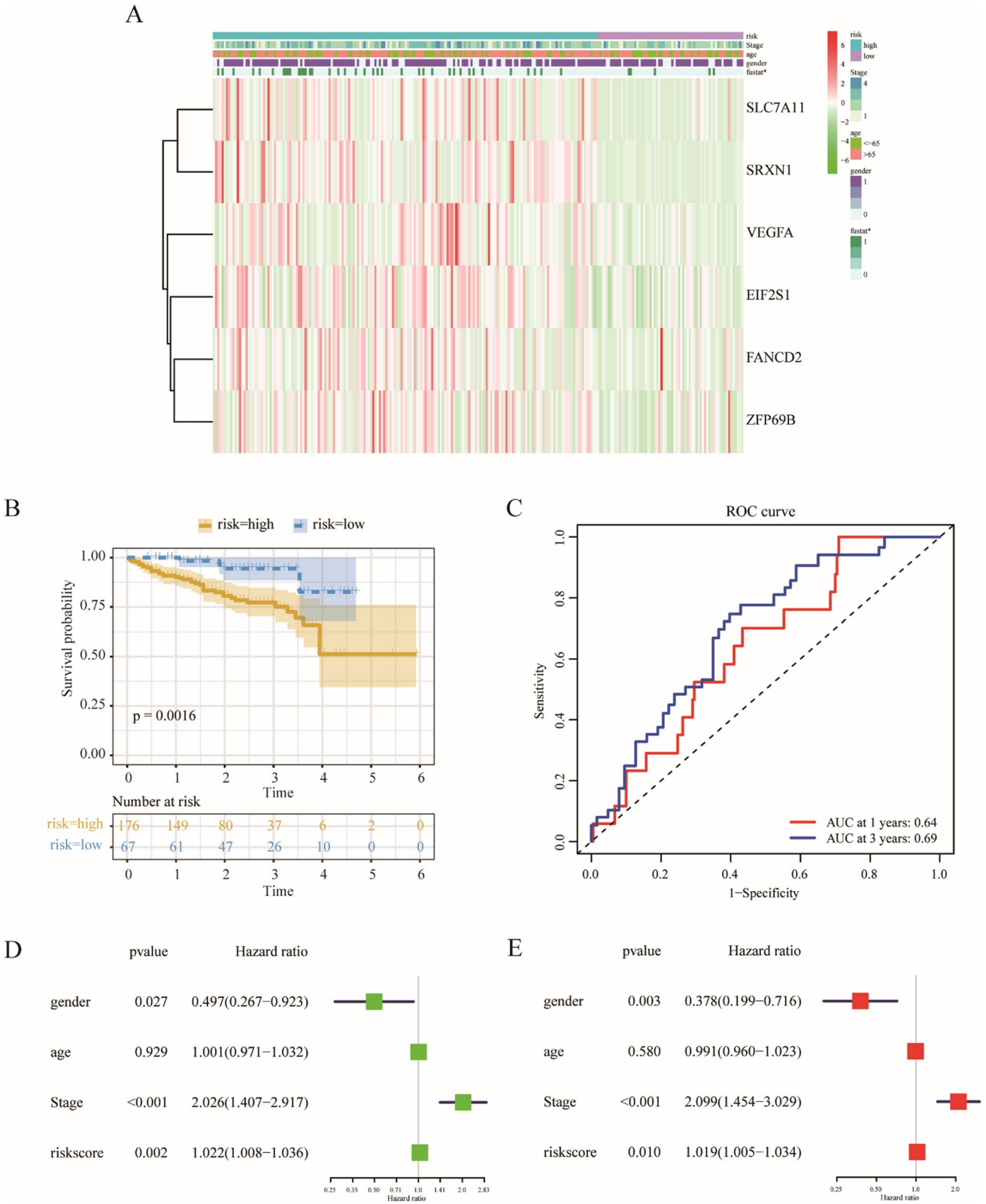

Fig. 7 Validation of m6A-FRGs by ICGC dataset. **A** The heatmap showed the expression of six genes in the ICGC dataset. **B** Kaplan–Meier plotter revealed that the high score of m6A-FRGs can predict the worse outcome of HCC patients in the ICGC dataset, *p* value was 0.0016. **C** the ROC curve of m6A-FRGs for diagnosing HCC. **D** Univariate and **E** multivariate Cox regression analyses for OS in HCC patients. Abbreviations: FRG, ferroptosis-related genes; ICGC, International Cancer Genome Consortium

Table 1 Correlation between ZFP69B expression and clinical characteristics in HCC (n = 144)

Clinical characteristics	ZFP69B expression		*P* value
	Low(N = 72)	High(N = 72)	
Sex (Female vs. male)			0.46
Female	11	8	
Male	61	64	
Age, year (≤ 50 vs. > 50)			0.095
≤ 50	29	39	
> 50	43	33	
AFP, ng/mL (≤ 13.4 vs. > 13.4)			**0.025**
≤ 13.4	33	20	
> 13.4	39	52	
HBsAg (negative vs. positive)			0.479
Negative	12	9	
Positive	60	63	
Liver cirrhosis (negative vs. positive)			0.643
Negative	10	12	
Positive	62	60	
Tumor size, cm (≤ 5 vs. > 5)			1.000
≤ 5 cm	38	38	
> 5 cm	34	34	
Tumor number (single vs. multiple)			0.248
Single	57	51	
Multiple	15	21	
Tumor encapsulation (complete vs. none)			0.284
Complete	52	46	
None	20	26	
Vascular invasion (negative vs. positive)			0.045
Negative	45	33	
Positive	27	39	
Tumor differentiation (I + II vs. III + IV)			0.298
I + II	49	43	
III + IV	23	29	
TNM stage (I vs. II + III)			**0.000**
I	41	20	
II and III	31	52	

AFP alpha-fetoprotein, *TNM* tumor-node-metastasis

Similar results were observed. Specifically, the ICGC dataset was used to independently verify the model. First, the expression levels of the six genes were significantly upregulated in the ICGC cohort, consistent with our previous findings. Although Kaplan–Meier survival analysis did not show a statistically significant difference in overall survival based on the m6A-FRGs score, univariate Cox regression analysis indicated that the signature had a significant association with patient prognosis. Furthermore, multivariate Cox regression confirmed that the m6A-FRGs signature served as an independent prognostic predictor. These results demonstrated the robust predictive performance of the m6A-FRGs model across two independent cohorts, supporting its stability and potential clinical utility.

Despite the promising results, several limitations should be acknowledged. First, our findings suggest that high-risk

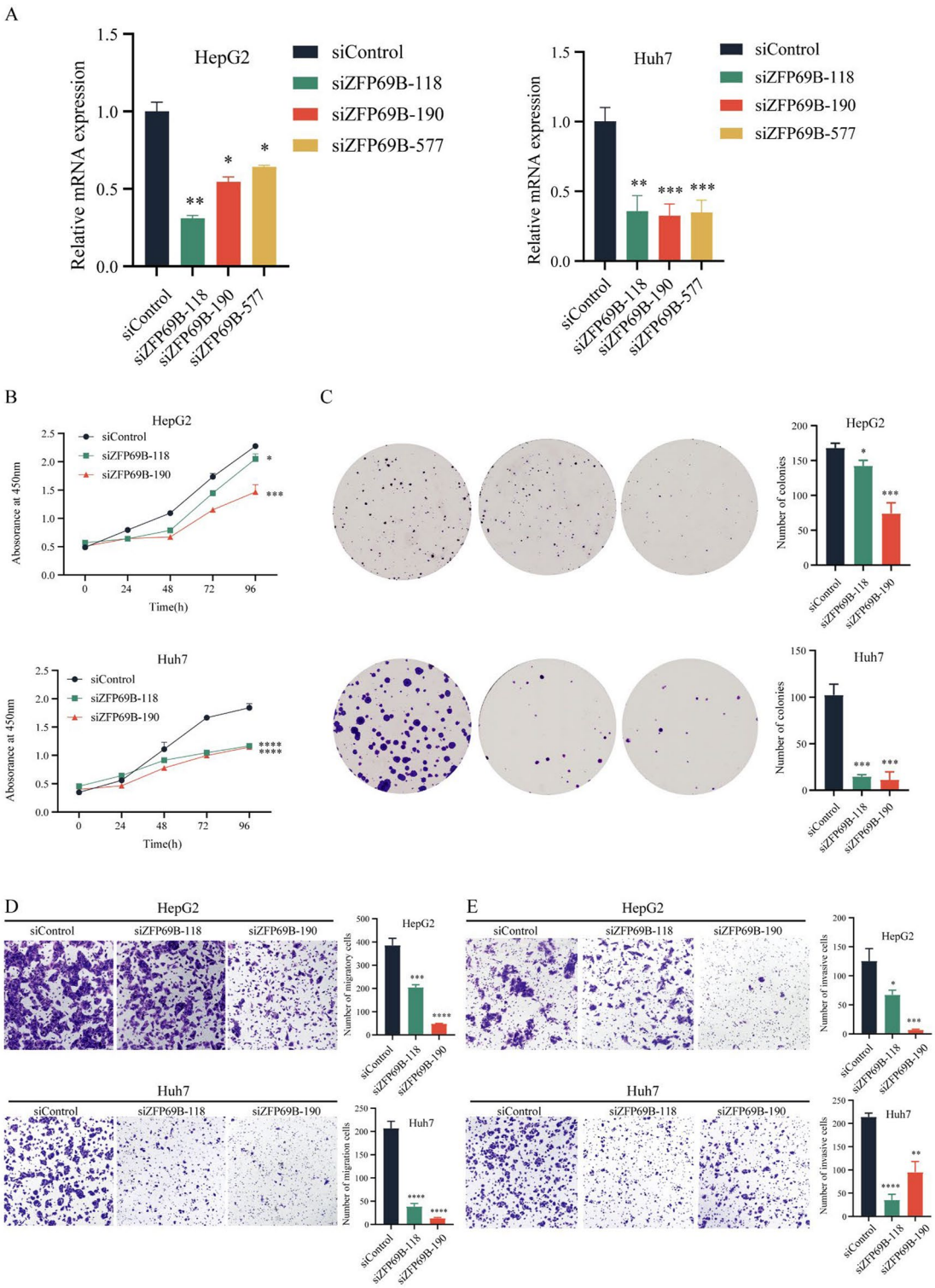

Fig. 8 Silencing ZFP69B inhibits the proliferation, migration and invasion of HCC cells in vitro. **A** The silencing of ZFP69B expression in HepG2 and Huh7 cells was confirmed by qRT-PCR. **B** The suppression of ZFP69B expression in HepG2 and Huh7 cells resulted in delayed cell proliferation, as assessed by the CCK-8 assay. **C** Colony formation assays demonstrated that inhibiting ZFP69B expression reduced the proliferation of HepG2 and Huh7 cells. **D** A migration assay was performed to evaluate the migratory capacity of HepG2 and Huh7 cells. The cells were fixed, stained with crystal violet, and representative images were captured. **E** An invasion assay was conducted to assess the invasive potential of HepG2 and Huh7 cells. Values are mean ± SEM. *: $P \leq 0.05$; **: $P \leq 0.01$; ***: $P \leq 0.001$; ****: $P \leq 0.0001$ ns: $P > 0.05$, Not significant. All experiments were performed in triplicate

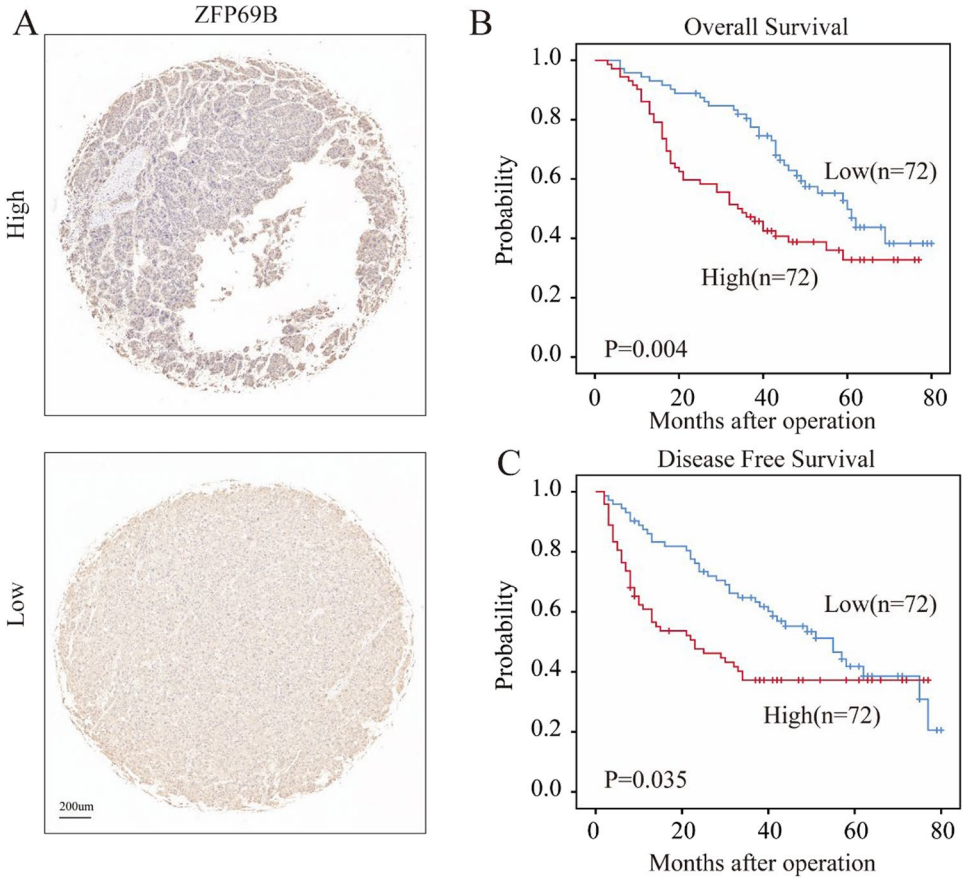

Fig. 9 Prognostic impact of ZFP69B expression status in liver cancer patients. **A** Representative images of ZFP69B expression in liver cancer samples from both high ZFP69B expression (n = 72) and low ZFP69B expression (n = 72) groups. **B** Patients with high expression of ZFP69B have a shorter overall survival (OS) period. **C** Patients with high expression of ZFP69B have a shorter Disease-free survival (DFS) period

patients may derive greater benefit from immunotherapy. However, the predictive value of this signature for immunotherapy response needs to be verified through clinical trials. To facilitate clinical implementation, one potential approach is to assess the expression of m6A-FRGs via qPCR using postoperative tissue samples. This would enable individualized prognostic prediction and allow clinicians to stratify patients based on their risk levels. For high-risk patients, more intensive follow-up strategies could be adopted to closely monitor disease progression and enable timely intervention. This personalized approach could ultimately help refine treatment strategies and improve clinical outcomes in HCC patients. Second, while the current findings underscore the significance of ZFP69B in predicting prognosis for HCC patients, further studies are required to investigate its role in ferroptosis and the impact of m6A modification on its expression and function. Third, while the clinical relevance of ZFP69B as a prognostic marker has been established, additional validation involving ferroptosis-related pathways and m6A-mediated regulatory mechanisms is essential to strengthen the overall prognostic utility of the model.

Conclusion

Taken together, we explored the role of m6A-modified FRGs in the prognosis of HCC by a variety of bioinformatics analyses. We developed and validated the prognostic m6A-FRGs model by LASSO. This model demonstrated good prognostic accuracy for 1-, 3-, and 5-year survival in HCC patients, with AUC values of 0.76, 0.68, and 0.66 at 1-, 3-, and 5-year survival, respectively. External databases further validated that m6A-FRGs was an independent predictor for prognosis of HCC. This novel comprehensive m6A-FRGs signature suggests that the individualized treatment should be adopted for HCC patients with different status. On the other hand, the m6A-FRGs model also implies that a ferroptosis inhibitor could synergize with m6A inhibitors to achieve better therapeutic outcomes. This comprehensive m6A-FRGs signature highlights the importance of individualized treatment approaches for HCC patients with varying clinical statuses. Furthermore, the key gene of m6A-FRGs, ZFP69B, inhibition of which may provide a novel therapeutic target for ferroptosis- related treatments.

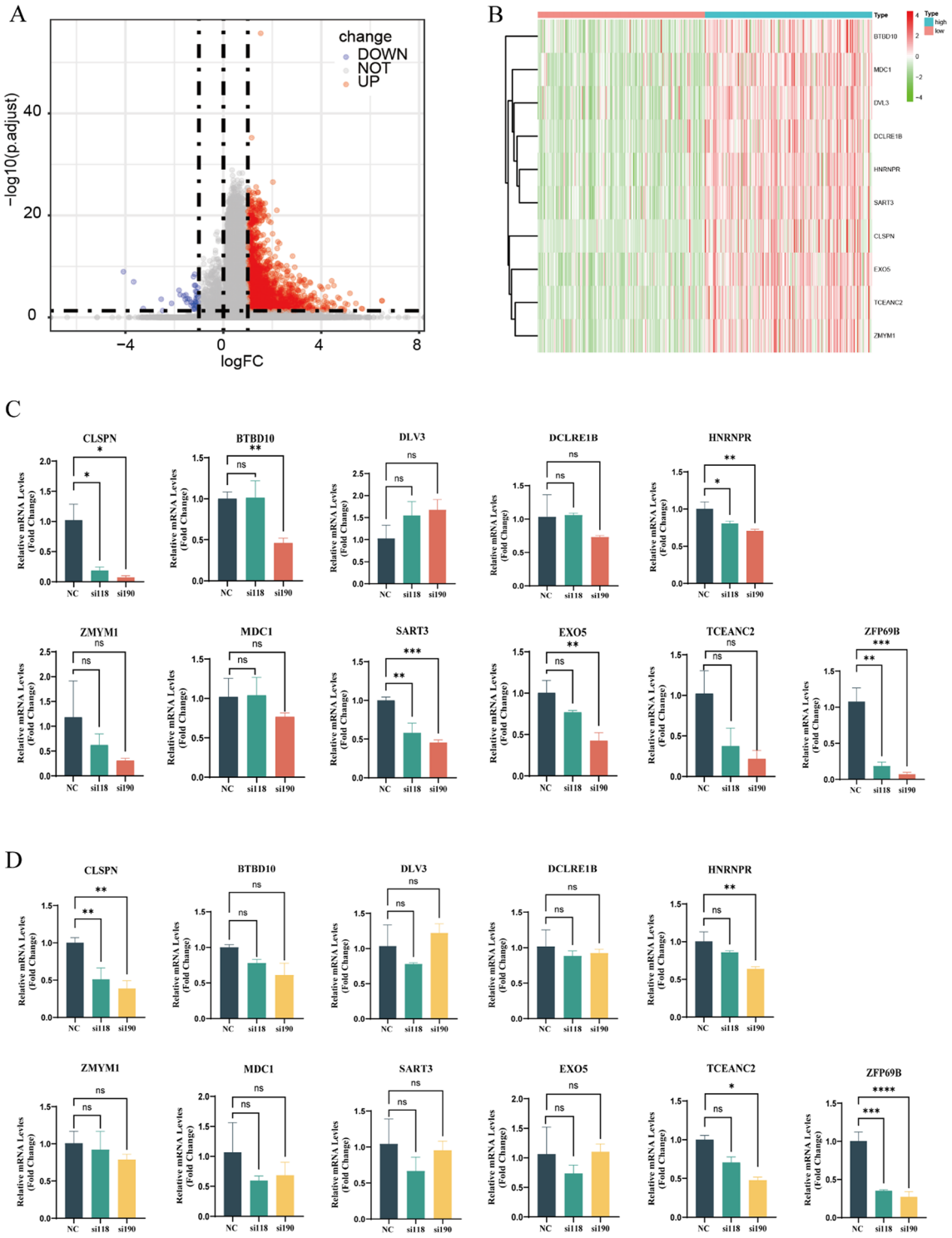

Fig. 10 Potential downstream genes of ZFP69B. **A** Volcano map. Differentially expressed genes between the two groups based on high and low expression of ZFP69B in 144 clinical samples. **B** Heatmap. The top ten genes (BTBD10, MDC1, DVL3, DCLRE1B, HNRNPR, SART3, CLSPN, EXO5, TCEANC2, and ZMYM1), selected based on the largest fold-change differences in the differentially expressed genes between the two groups, were identified by comparing high and low expression of ZFP69B in clinical samples. **C** After silencing ZFP69B in Huh7 cells, the expression changes of these potential downstream genes (BTBD10, MDC1, DVL3, DCLRE1B, HNRNPR, SART3, CLSPN, EXO5, TCEANC2, and ZMYM1) were observed. **D** Following the knockdown of ZFP69B in HepG2 cells, alterations in the expression levels of these potential downstream genes (BTBD10, MDC1, DVL3, DCLRE1B, HNRNPR, SART3, CLSPN, EXO5, TCEANC2, and ZMYM1) were detected

Supplementary Information The online version contains supplementary material available at https://doi.org/10.1007/s10238-025-01700-4.

Author contributions YH, ZLZ, and ZYL contributed to the study design. MC, XZ, and RSL were primarily responsible for data collection, analysis, and manuscript revision. YH, ZYL, and WZ performed the experiments. GTZ TW and ERC was responsible for the study concept and design. EBC contributed to the study supervision, data analysis, and manuscript writing. All authors read and approved the final manuscript.

Funding This work was supported by the National Natural Science Foundation of China (82303446), GuangDong Basic and Applied Basic Research Foundation (2023A1515220200), Medical Scientific Research Foundation of Guangdong Province of China (A2024351), Science and Technology Development Fund Project of Shenzhen (JCYJ20240813115900001) and Shenzhen High-level Hospital Construction Fund, and Peking University Shenzhen Hospital Scientific Research Fund (KYQD2023303), Hubei Provincial Natural Science Foundation (2024AFB531).

Data availability All date and materials are available from the corresponding authors upon request.

Declarations

Conflict of interest The authors declare that they have no conflict of interest.

References

1. Villanueva A. Hepatocellular carcinoma. N Engl J Med. 2019;380(15):1450–62.
2. Chen W, et al. Cancer statistics in China, 2015. CA Cancer J Clin. 2016;66(2):115–32.
3. Komatsu S, et al. Treatment outcomes of hepatectomy and systemic chemotherapy based on oncological resectability criteria for hepatocellular carcinoma. Ann Gastroenterol Surg. 2025;9(2):235–43.
4. Di Federico A, et al. Atezolizumab-bevacizumab plus Y-90 TARE for the treatment of hepatocellular carcinoma: preclinical rationale and ongoing clinical trials. Expert Opin Investig Drugs. 2022;31(4):361–9.
5. Carloni R, et al. Immune-based combination therapies for advanced hepatocellular carcinoma. J Hepatocell Carcinoma. 2023;10:1445–63.
6. Sahin TK, et al. Prognostic value of neutrophil-to-eosinophil ratio (NER) in cancer: a systematic review and meta-analysis. Cancers (Basel). 2024;16(21):3689.
7. Luo Y, et al. Autophagy-related gene pairs signature for the prognosis of hepatocellular carcinoma. Front Mol Biosci. 2021;8:670241.
8. Hong L, et al. A stemness-based eleven-gene signature correlates with the clinical outcome of hepatocellular carcinoma. BMC Cancer. 2021;21(1):716.
9. Chen C, et al. Five metastasis-related mRNAs signature predicting the survival of patients with liver hepatocellular carcinoma. BMC Cancer. 2021;21(1):693.
10. Chen XY, Zhang J, Zhu JS. The role of m(6)A RNA methylation in human cancer. Mol Cancer. 2019;18(1):103.
11. Balacco DL, Soller M. The m(6)A writer: rise of a machine for growing tasks. Biochemistry. 2019;58(5):363–78.
12. Wang S, et al. Novel insights on m(6)A RNA methylation in tumorigenesis: a double-edged sword. Mol Cancer. 2018;17(1):101.
13. Li Q, et al. HIF-1alpha-induced expression of m6A reader YTHDF1 drives hypoxia-induced autophagy and malignancy of hepatocellular carcinoma by promoting ATG2A and ATG14 translation. Signal Transduct Target Ther. 2021;6(1):76.
14. Chen M, et al. RNA N6-methyladenosine methyltransferase-like 3 promotes liver cancer progression through YTHDF2-dependent posttranscriptional silencing of SOCS2. Hepatology. 2018;67(6):2254–70.
15. Chen Y, et al. ALKBH5 suppresses malignancy of hepatocellular carcinoma via m(6)A-guided epigenetic inhibition of LYPD1. Mol Cancer. 2020;19(1):123.
16. Hou W, et al. Autophagy promotes ferroptosis by degradation of ferritin. Autophagy. 2016;12(8):1425–8.
17. NaveenKumar SK, et al. The role of reactive oxygen species and ferroptosis in heme-mediated activation of human platelets. ACS Chem Biol. 2018;13(8):1996–2002.
18. Jiang L, et al. Ferroptosis as a p53-mediated activity during tumour suppression. Nature. 2015;520(7545):57–62.
19. Hattori K, et al. Cold stress-induced ferroptosis involves the ASK1-p38 pathway. EMBO Rep. 2017;18(11):2067–78.
20. Yao X, et al. Simvastatin induced ferroptosis for triple-negative breast cancer therapy. J Nanobiotechnol. 2021;19(1):311.
21. Deng S, et al. M6A2Target: a comprehensive database for targets of m6A writers, erasers and readers. Brief Bioinform. 2021;22(3):bbaa055.
22. Zhou N, Bao J. FerrDb: a manually curated resource for regulators and markers of ferroptosis and ferroptosis-disease associations. Database (Oxford). 2020;2020:baaa021.
23. Bagaev A, et al. Conserved pan-cancer microenvironment subtypes predict response to immunotherapy. Cancer Cell. 2021;39(6):845–65.
24. Chen EB, et al. The miR-561–5p/CX(3)CL1 signaling axis regulates pulmonary metastasis in hepatocellular carcinoma involving CX(3)CR1(+) natural killer cells infiltration. Theranostics. 2019;9(16):4779–94.
25. Liu P, et al. Establishment of a prognostic model for hepatocellular carcinoma based on endoplasmic reticulum stress-related gene analysis. Front Oncol. 2021;11:641487.
26. Dey S, Tameire F, Koumenis C. PERK-ing up autophagy during MYC-induced tumorigenesis. Autophagy. 2013;9(4):612–4.
27. de Oliveira A, et al. Differential expression of angiogenesis-related miRNAs and VEGFA in cirrhosis and hepatocellular carcinoma. Arch Med Sci. 2020;16(5):1150–7.

28. Palagyi A, et al. Genetic inactivation of the Fanconi anemia gene FANCC identified in the hepatocellular carcinoma cell line HuH-7 confers sensitivity towards DNA-interstrand crosslinking agents. Mol Cancer. 2010;9:127.
29. Bi F, et al. METTL9-SLC7A11 axis promotes hepatocellular carcinoma progression through ferroptosis inhibition. Cell Death Discov. 2023;9(1):428.
30. Zheng X, et al. Construction and analysis of the tumor-specific mRNA-miRNA-lncRNA network in gastric cancer. Front Pharmacol. 2020;11:1112.